

Neuron, Volume 59

Supplemental Data

High-Resolution Intracellular Recordings Using a Real-Time Computational Model of the Electrode

**Romain Brette, Zuzanna Piwkowska, Cyril Monier, Michelle Rudolph-Lilith, Julien Fournier,
Manuel Levy, Yves Frégnac, Thierry Bal, and Alain Destexhe**

High-resolution intracellular recordings using a real-time interaction between the neuron and a computational model of the electrode

Supplementary Methods

R. Brette, Z. Piwkowska, C. Monier, M. Rudolph-Lilith, J. Fournier, M. Levy, Y. Frégnac, T. Bal, A. Destexhe

Contents

| | | |
|----------|--|-----------|
| 1 | Biological preparation | 2 |
| 2 | Electrophysiology | 2 |
| 3 | Data analysis | 3 |
| 3.1 | White noise injection | 3 |
| 3.2 | Square conductance pulses | 3 |
| 3.3 | Colored conductance noise | 5 |
| 3.4 | Spike onset analysis | 5 |
| 3.5 | Spike shape analysis | 6 |
| 4 | Theoretical analysis of dynamic clamp errors | 7 |
| 4.1 | Steady-state errors resulting from poor electrode compensation . . | 7 |
| 4.2 | Instabilities with bridge compensation | 7 |
| 4.3 | Instabilities induced by digital sampling | 9 |
| 5 | Kernel estimation | 10 |
| 5.1 | The least square problem | 10 |
| 5.2 | Fast implementation | 11 |
| 5.3 | Choosing the input signal | 12 |
| 5.4 | Isolation of electrode kernel | 14 |
| 5.5 | Implementation | 17 |
| 6 | Typical sources of error | 18 |

1 Biological preparation

All research procedures concerning the experimental animals and their care adhered to the American Physiological Society's Guiding Principles in the Care and Use of Animals, to the European Council directive 86/609/EEC and to European Treaties Series 123 and was also approved by the local ethics committee "Ile-de-France Sud" (Certificate 05-003).

2 Electrophysiology

Sharp electrodes for intracellular recordings were made on a Sutter Instruments P-87 micropipette puller from medium-walled glass (WPI, 1BF100) and bevelled on a Sutter Instruments beveller (BV-10M). Micropipettes were filled with 1.2-2 M potassium acetate - 4 mM potassium chloride and had resistances of 65-110 M Ω after bevelling. An Axoclamp 2B amplifier (Axon Instruments) was used for V_m recording and current injection. A Digidata 1322A card (Axon Instruments) and the PC-based software ELPHY (developed by G. Sadoc, CNRS Gif-sur-Yvette, ANVAR and Biologic) were used for data acquisition at 20 kHz. The Axoclamp was used either in continuous current-clamp ('bridge') mode or in discontinuous current-clamp (DCC) mode. In both cases, the capacitance neutralization was set at the maximal possible value, slightly before the onset of oscillations, to achieve the fastest possible electrode charging time (as assessed by the Monitor output viewed at high temporal resolution on an analogical oscilloscope, allowing to adjust the time constant of the electrode response decay after injection of ultra-short current pulses in discontinuous mode). The switching frequency of the DCC mode was chosen accordingly, so that the sampling of the V_m took place after the electrode transient had decayed to a plateau (http://www.moleculardevices.com/pages/instruments/axon_guide.html).

In both the continuous current-clamp ('bridge') mode and the discontinuous current-clamp (DCC) mode of the Axoclamp, the maximal possible capacitance neutralization was carefully set slightly before the onset of oscillations, to achieve the fastest possible electrode charging time. This setting was assessed by viewing the Monitor output of the Axoclamp at high temporal resolution on an analogical oscilloscope: this allows the precise adjustment of the time constant of the electrode response decay after injection of ultra-short current pulses in discontinuous mode. We always made sure that this decay remained monotonous, without over- or undershoots indicating the onset of dampened oscillations due to capacitance over-compensation. The switching frequency of the DCC mode was chosen accordingly, so that the sampling of the V_m took place after the electrode transient had decayed to a plateau. This is the standard procedure described in the Axoclamp manual (http://www.moleculardevices.com/pages/instruments/axon_guide.html). In addition, the presence of undesirable oscillations between injected current and V_m could also readily be detected at the level of the elec-

trode kernel (see Supplementary Figure 5a): after each estimation, we inspected the kernel to check for remaining dampened oscillations, and reduced the capacitance neutralization setting until these were no longer present (Supplementary Figure 5b).

3 Data analysis

The PC-based software ELPHY (developed by G. Sadoc, CNRS Gif-sur-Yvette, ANVAR and Biologic), Matlab (The Mathworks, Natick, MA) , Scilab (INRIA / ENPC, <http://www.scilab.org>) and custom-written C-code were used. All statistical tests were performed using the software Statview 5.0 (SAS Institute, Cary, N.C.). All values are given as average \pm standard deviation or, for small sample size, as average and range. A P-value < 0.05 was required for statistical significance.

3.1 White noise injection

Since the injected subthreshold current noise had a mean of 0 nA, we only compared the standard deviations of recorded V_m distributions with theoretical values of standard deviations predicted from the noise parameters and passive neuron parameters derived from responses to small current pulses. Relative error is:

$$100 \times \frac{|\sigma_{\text{experiment}} - \sigma_{\text{theory}}|}{\sigma_{\text{theory}}}$$

and

$$\sigma_{\text{theory}} = R \sqrt{\frac{dt}{2\tau_m}} \sigma_I$$

where R is the input resistance, τ_m is the membrane time constant, dt is time step (0.1 ms in our experiments) and σ_I is the standard deviation of the input current (for a single sampling step).

3.2 Square conductance pulses

For each train of injected pulses, an initial stable part of the response was selected for analysis (as assessed by a non-significant Spearman non-parametric test for correlation between response amplitude and time), in order to minimize deviations from the theoretical prediction due to small drifts in the recording.

Recordings were analyzed on phase plots of $V_m(t + T/4)$ vs. $V_m(t)$ (where T is the period of the waveform), where predicted responses for a passive membrane are squares. We fit an optimal square to the experimental phase plot (least square minimization of the average distance of experimental points to the square), then compared the length of the side and the tilt between the optimal square and the theoretical square (equations below). The level of noise in the experimental trace

was quantified by the average distance (in mV) of the data points to the optimal square.

In each cell, a given parameter configuration is always tested in both AEC and DCC. Differences between the two conditions are thus tested with a paired statistical test, the Wilcoxon non-parametric test. Correlations between measures derived from the phase plots and stimulus parameters were evaluated using simple linear regression analysis: the P-values given correspond to the null hypothesis that the slope of the linear regression is 0 (two-tailed t-test). For descriptive statistics and linear regression analyses, one data point was excluded (for both methods and all error measures): given the very small theoretical prediction for the side measure, in one case of 1000 Hz stimulus frequency, the relative error on the side measure was extremely large (due to division by this very small value) and constituted a clear outlier. The removal of this one point did not affect the results of the Wilcoxon tests nor of most linear regression analyses.

Response of a passive membrane to square conductance pulses

We consider a passive membrane model with a square conductance wave stimulation described by the following equation:

$$C \frac{dV_m}{dt} = -g_L(V_m - V_{\text{rest}}) - g^+(t)(V_m - E^+) - g^-(t)(V_m - E^-)$$

where C is the membrane capacitance, g_L is the leak conductance ($1/R$), E^+ and E^- are reversal potentials, and $g^+(t)$ and $g^-(t)$ are time-varying conductances. The conductances are alternating square pulses, i.e., $g^+(t) = g$ and $g^-(t) = 0$ when $t \bmod T \in [0, T/2[$, and $g^-(t) = g$ and $g^+(t) = 0$ when $t \bmod T \in [T/2, T[$, where T is the period and g is the maximum conductance.

Because the total conductance $g + g_L$ is constant, the response $V_m(t)$ is piecewise exponential with time constant $(g + g_L)/C$. After the response settles in the stationary regime, it is periodic (period of the stimulus T) and consists of an alternation of two pieces of exponential functions, of the form $a + b \exp(-(g + g_L)t/C)$. It follows for any given delay d , $V(t + d)$ and $V(t)$ are related by an affine relation on every smooth piece, and there are $2 \times 2 = 4$ different sets of parameters. Therefore the phase plot defined by the graph of $(V(t), V(t + d))$ is a quadrilateral. When $d = T/4$, symmetry arguments imply that it must be square.

The corners of the square correspond to the discontinuity points of the conductance pulses. Solving the differential equation gives an explicit formula for their coordinates. The coordinates of the center of the square are

$$(C_x, C_y) = \left(\frac{g}{g + g_L} \frac{E^+ E^-}{2}, \frac{g}{g + g_L} \frac{E^+ E^-}{2} \right)$$

and the coordinates of the first corner are

$$(M_x, M_y) = \left(C_x + \frac{A}{2}, C_y + \frac{A}{2(1 + \alpha)} \right)$$

where

$$A = \frac{g}{g + g_L} (E^+ - E^-) \frac{1 - \alpha^2}{1 + \alpha^2}$$

$$\alpha = \exp\left(-\frac{(g + g_L)T}{4C}\right)$$

The three other corners are obtained by rotations around the center C with angles of 90° , 180° and 270° .

3.3 Colored conductance noise

Fragments of responses to fluctuating conductance injection (see [4] for stochastic equations generating these conductances; parameters used here were similar) were selected so as to avoid rare spikes or rare, very sharp electronic artefacts (seen in some recordings independent of compensation method or protocol used) which introduce spurious high frequencies. V_m distributions were obtained for each fragment and their parameters were averaged over fragments. Theoretical V_m distributions were computed using a steady-state solution of the passive membrane equation (see [1] for equations) and known injected conductance and passive membrane parameters (derived from response to small current pulses). The difference between theory and experiment was quantified by the relative error:

$$100 \times \frac{|\text{param}_{\text{experiment}} - \text{param}_{\text{theory}}|}{\text{param}_{\text{theory}}}$$

The Wilcoxon test was used to assess whether the relative errors for AEC and for DCC were significantly different. Each fragment was also fit by the theoretical template of the PSD [5] using a simplex fitting algorithm [6]. The theoretical template was:

$$S_V(\omega) = \frac{1}{1 + \omega^2 \tilde{\tau}_m^2} \left[\frac{A_e \tau_e}{1 + \omega^2 \tau_e^2} + \frac{A_i \tau_i}{1 + \omega^2 \tau_i^2} \right]$$

where $\omega = 2\pi f$, f is the frequency, $\tilde{\tau}_m$ is the effective membrane time constant, A_e and A_i are amplitude parameters and τ_e and τ_i time constants for excitation and inhibition, respectively. Fits were realized by fitting both A_e and A_i , as well as τ_e and τ_i . $\tilde{\tau}_m$ was fixed to the value estimated from the recordings. Different initial conditions (“first guesses”) were given to the fitting procedure to ensure that there was no convergence to local minima. Fit errors were averaged over fragments (Fig. 5f).

3.4 Spike onset analysis

Spikes were triggered by a realistic dynamic-clamp 300s-long protocol combining randomized injection of AMPA synaptic inputs of 5 different amplitudes at 10 Hz

and injection of a background of colored conductance noise [4] in either a “high conductance” ($g_i > g_e$), or a “low conductance” configuration ($g_e = g_i$) (Z.P. et al, <http://arxiv.org/abs/0706.1306>). For each injection protocol, an initial stable part of the response was selected for analysis (as assessed by a non-significant Spearman non-parametric test for correlation between spike threshold and time). 914 spikes were analyzed on average for each protocol (range 251-1895 spikes). Both AMPA-triggered and spontaneous spikes were analyzed together. The threshold of each spike was detected whenever the difference between two consecutive data points first exceeded 4 mV (corresponding to a threshold of around 80 mV/ms on the derivative of the V_m ; this procedure is similar to [7]). A lower value of 2 mV for this difference also provided threshold detection in good correspondence with visual detection on AEC recordings; in this case, a significant negative correlation between depolarization slope and threshold was found as well (average slope of linear regression: -1.6 ms, range -3.5 to -0.7 ms; average coefficient of regression: 0.582, range 0.437 to 0.72). However, this lower value did not ensure proper spike threshold detection in DCC (spurious spike detection) nor in smoothed DCC (undetected spikes). The smoothed DCC trace was obtained by replacing each data point i by the average of 9 surrounding points (i.e. an average from $i - 4$ to $i + 4$). The 9-point size of the sliding window was chosen by visual inspection of the resulting trace in order to produce spikes that maximally resemble the spikes recorded in AEC. The slope of the depolarization preceding the spike is computed by a linear regression on 50 data points (2.4 ms) before the spike (excluding the data point at which the threshold is detected). We found that for this duration, the linear fit constituted a good approximation of the rise of the V_m before the spike on a trial by trial basis, for both low conductance and high conductance states. For longer durations, increasing V_m fluctuations reduced the accuracy of the linear fit. We verified however that a significant correlation between the slope of the linear regression and the V_m at spike threshold could also be established for longer time windows: the maximal duration for which this correlation could be retained ranged from 4 to 7 ms for high conductance states, and from 6 to 10 ms for low conductance states. Both a linear and an exponential function were fit to the clouds of points representing the threshold of each spike as a function of the slope of the preceding depolarization. The exponential fits were in some cases slightly better than the linear ones, but in other cases they were indistinguishable: since in those cases the time constants of the exponential fits have aberrant values, the exponential fits were not analyzed further. The significance of the correlation between slope of depolarization and spike threshold was assessed using a non-parametric Spearman correlation test.

3.5 Spike shape analysis

Spike threshold is detected as above, using a threshold difference of 2 mV between two successive data points. Spike height is the maximal V_m during the spike minus the V_m at threshold. Spike width is measured half-way between the threshold and

the maximal V_m .

4 Theoretical analysis of dynamic clamp errors

In this section we analyse the errors and instabilities that can result from incomplete electrode compensation in dynamic clamp protocols. We consider a simple protocol where the current $I = g(E - V)$ is injected, where g is a constant conductance, E is a constant potential and V is the estimated membrane potential V_m . The membrane is modeled as an electrical circuit with resistance R and capacitance C (the resting potential is chosen to be 0 mV).

4.1 Steady-state errors resulting from poor electrode compensation

At equilibrium, the recording potential before compensation is $V_r = V_m + R_e I$ (by definition of the electrode resistance, independently of its properties). If the estimated electrode resistance is $R_e + \Delta R_e$ (whether by bridge compensation or AEC), then the estimated potential is $V = V_m + \Delta R_e I = (R + \Delta R_e)g(E - V)$, thus

$$V = \frac{(R + \Delta R_e)gE}{1 + (R + \Delta R_e)g}$$

which can be expressed as follows: the dynamic clamp interprets the residual electrode resistance as part of the membrane resistance. The membrane resistance is

$$V_m = RI = gR(E - V) = \frac{gRE}{1 + (R + \Delta R_e)g}$$

Therefore the relative error (compared to the case $\Delta R_e = 0$) is

$$\begin{aligned} \frac{V_m}{V_m^*} - 1 &= \frac{1 + gR}{1 + (R + \Delta R_e)g} - 1 \\ &= -\frac{\Delta R_e g}{1 + (R + \Delta R_e)g} \\ &\approx -\Delta R_e g \end{aligned}$$

(for small error ΔR_e). For large clamp conductance g , the relative error tends to $-\Delta R_e/(R + \Delta R_e)$.

4.2 Instabilities with bridge compensation

We consider a dynamic clamp protocol with ideal bridge compensation, i.e., $V = V_r - R_e I$, where R_e is the (perfectly estimated) electrode resistance. The dynamic clamp is analog, so that there is no feedback delay. The electrode is modeled as a resistor (R_e) and a capacitor (C_e). In the absence of the capacitor, the bridge estimation is perfect, i.e., $V = V_m$, otherwise it differs from the real membrane

potential because of the capacitive current through the electrode. The dynamic clamp current is $I = g(E - V_r - R_e I)$, thus:

$$I = \frac{g(E - V_r)}{1 - gR_e} = \alpha(E - V_r)$$

where α is a definition. We already note that $\alpha < 0$ if and only if $gR_e < 1$, which, as we will see, is the stability condition. In the following we consider Laplace transforms of the time-dependent variables. With the Laplace variable s , the impedance of a capacitor is $1/(Cs)$. The current flowing through the electrode is the command current minus the current flowing through the electrode capacitance:

$$I_e = I - C_e s V_r = \alpha(E - V_r) - C_e s V_r \quad (1)$$

It also equals the transmembrane current:

$$I_e = (R_m^{-1} + Cs)V_m = (R_m^{-1} + Cs)(V_r - R_e I_e)$$

and thus

$$I_e = \frac{(R_m^{-1} + Cs)V_r}{1 + (R_m^{-1} + Cs)R_e} \quad (2)$$

From equations (1) and (2), it follows:

$$(R_m^{-1} + Cs)V_r = (\alpha(E - V_r) - C_e s V_r)(1 + (R_m^{-1} + Cs)R_e)$$

The solutions are stable if and only if the roots of the following polynomial have a negative real part:

$$R_m^{-1} + Cx + (\alpha + C_e x)(1 + (R_m^{-1} + Cx)R_e)$$

This is equivalent to the statement that the sum of the roots is negative and their product is positive, that is:

$$\begin{aligned} C(\alpha R_e + 1) + C_e(1 + R_m^{-1} R_e) &> 0 \\ R_m^{-1} + \alpha(1 + R_m^{-1} R_e) &> 0 \end{aligned}$$

If $\alpha > 0$, this is clearly true. Conversely, the second inequality can be re-expressed as $1 + \alpha(R_m + R_e) > 0$, and using the formula for α :

$$\frac{1 + gR_m}{1 - gR_e} > 0$$

which is true if and only if $gR_e < 1$ (i.e., $\alpha > 0$).

Thus, the condition for stability with ideal bridge compensation is $gR_e < 1$. There is no ringing in this case, it only occurs when feedback delays are introduced (see next paragraph). To compare with the stability condition in the next section, it is useful to write this condition as follows:

$$gR < \frac{R}{R_e}$$

In our experiments (with high resistance electrodes), this ratio was between 0.3 and 1, and in that case only conductances smaller than the membrane conductance can be injected. When the electrode is correctly compensated, the limiting factor is the feedback delay, as explained below, and the critical clamp conductance is much higher.

In the derivation of the critical conductance, we modeled the electrode resistance as a simple RC circuit, with the capacitor on the amplifier side. If the capacitance is distributed, the result would change slightly; for example if the capacitor is moved to the middle of the resistor, then the critical conductance will be twice higher (because half of the resistance if fully compensated).

4.3 Instabilities induced by digital sampling

Here we study the effect of digital sampling for the dynamic clamp with an otherwise ideal setup with perfect electrode compensation. A computer or a digital signal processor records and injects at sampling rate f . At time $t_n = n/f$, the membrane potential $V_n = V(t_n)$ is sampled, then the computer calculates the current to inject $I_n = g(E - V_n)$ during the interval $[t_n, t_{n+1}[$, and the current is injected during the next interval $[t_{n+1}, t_{n+2}[$. (hence the feedback delay is $2/f$). Assuming perfect electrode compensation (i.e., in effect, no electrode), the dynamics of the sampled membrane potential is given by the following recurrence equation:

$$\begin{aligned} V_{n+2} &= \lambda V_{n+1} + (1 - \lambda)RI_n \\ &= \lambda V_{n+1} + (1 - \lambda)gR(E - V_n) \end{aligned}$$

where $\lambda = \exp(-1/\tau f) \in]0, 1[$ ($\tau = RC$ is the membrane time constant). In general the sampling step is at least two orders of magnitude smaller than the membrane time constant, so that $\lambda \approx 1 - 1/(\tau f)$. This is a second order linear recurrence equation, and the solutions are determined by the roots of the polynomial $X^2 - \lambda X + (1 - \lambda)gR$.

Oscillations can arise if the discriminant is negative, i.e., $\lambda^2 - 4(1 - \lambda)gR < 0$, which is approximately (using $1/f \ll \tau$):

$$gR > \frac{\tau f}{4}$$

In this case the real part of the roots is $-\lambda/2$, which is smaller than one, so that the solution of the recurrence equation is a damped oscillation, i.e., ringing.

If the discriminant is positive, then there are two real roots a and b , such that $a + b = \lambda \in]0, 1[$ and $ab = (1 - \lambda)gR > 0$. The latter inequality means that a and b have the same sign, and $a + b > 0$ implies that this sign is positive. From the inequality $a + b < 1$, it follows that a and b are both in $]0, 1[$, therefore the solutions of the recurrence equation are stable.

Thus, in the case of perfect compensation, the feedback delay induces ringing if $gR > \tau f/4$ but does not destabilise the system for constant conductances. In

our experiments, $\tau f \approx 100$, so that the maximum clamp conductance is about 25 times the membrane conductance.

Note that this inequality also applies to the maximal feedback gain of a digital voltage-clamp system (the expression we obtained is very similar to the formula derived by Finkel and Redman [8] in the analysis of the discontinuous voltage-clamp: $g_c = \tau f / (RD)$, where D is the duty cycle).

5 Kernel estimation

5.1 The least square problem

We assume that the neuron and the electrode respond linearly to the injected currents we use. We will discuss this hypothesis later. Then the recorded potential V in response to an input current I is the linear convolution:

$$V(t) = V_0 + (K * I)(t) = V_0 + \int_0^{+\infty} K(s)I(t-s)ds$$

where K is the impulse response of the system (neuron + electrode), also named the *kernel*, and V_0 is the resting potential. In the digital domain, the formula reads

$$V_n = V_0 + \sum_0^{+\infty} K_p I_{n-p}$$

Note that both the continuous and the discrete formulas express the linearity of the response and $V(t_n) = V_n$, but the continuous and discrete kernels are generally not identical. For example, the continuous kernel associated to an electrical circuit consisting of a resistance R and a capacitance C is $K(t) = (1/C) \exp(-t/RC)$, while its discrete kernel is $K'_n = (R/a) \exp(-ndt/RC)$, with $a = 1 - \exp(-dt/RC)$ (dt is the time step). The two kernels are equivalent for very small time steps dt .

If the time-varying current I is known and V is measured over a long enough period of time, then it is possible to calculate the kernel K . Assuming that the measure is corrupted by gaussian noise, the best estimation of K is the solution of the linear least square problem, i.e., (\mathbf{K}, V_0) minimizes

$$E = \sum_{n=0}^{N-1} \left(V_n - V_0 - \sum_{p=0}^{+\infty} K_p I_{n-p} \right)^2$$

where N is the number of measurements, i.e., $N\Delta$ is the duration of the stimulation, where Δ is the sampling step ($\Delta = 0.1$ ms in our experiments). Typically, the stimulation lasts 5 to 20 s, which corresponds to 50000 – 200000 measurements.

From $\frac{\partial E}{\partial V_0} = 0$ and $\frac{\partial E}{\partial K_i} = 0$ for all i we find:

$$\begin{aligned} \forall i \geq 0, \sum_{n=0}^{N-1} V_n I_{n-i} &= \sum_{p=0}^{+\infty} K_p \sum_{n=0}^{N-1} I_{n-p} I_{n-i} + V_0 \sum_{n=0}^{N-1} I_{n-i} \\ \sum_{n=0}^{N-1} V_n &= \sum_{p=0}^{+\infty} K_p \sum_{n=0}^{N-1} I_{n-p} + NV_0 \end{aligned}$$

with the convention $I_k = 0$ when $k < 0$ (no input current before time 0). In the following we define $\langle x_n \rangle = \frac{1}{N} \sum_{n=0}^{N-1} x_n$ (average over all samples).

In practice, we consider only the first M steps of the kernel K , so that the equations above can be expressed as a matrix problem $\mathbf{A}\mathbf{X} = \mathbf{B}$, where \mathbf{A} is a square matrix with coefficients $a_{i,j} = \langle I_{n-j} I_{n-i} \rangle$ for $i, j \in \{0 \dots M-1\}$, $a_{i,M} = \langle I_{n-i} \rangle$ for $i \in \{0 \dots M-1\}$, $a_{M,j} = \langle I_{n-j} \rangle$ for $j \in \{0 \dots M-1\}$ and $a_{M,M} = 1$; \mathbf{X} is a column vector with $X_i = K_i$ for $i \in \{0 \dots M-1\}$ and $X_M = V_0$; \mathbf{B} is a column vector with $B_i = \langle V_n I_{n-i} \rangle$ for $i \in \{0 \dots M-1\}$ and $B_M = \langle V_n \rangle$. Solving this linear equation for \mathbf{X} gives the coefficients of the kernel K and the resting potential V_0 .

5.2 Fast implementation

Although there is no theoretical problem in solving the linear problem described above, the matrix \mathbf{A} can be large and each coefficient $a_{i,j}$ is a sum over all samples. But we note that in the limit $N \rightarrow +\infty$ (infinite number of samples) $\langle I_{n-i} I_{n-j} \rangle = \langle I_n I_{n+i-j} \rangle$ for a stationary current. In this case the matrix \mathbf{A} has only $M+1$ distinct coefficients. However in practice the number of samples is finite, so that for $j > i$,

$$\begin{aligned} \langle I_{n-i} I_{n-j} \rangle &= \frac{1}{N} \sum_{n=-i}^{N-1-i} I_n I_{n+i-j} \\ &= \langle I_n I_{n+i-j} \rangle - \frac{1}{N} \sum_{n=N-i}^{N-1} I_n I_{n+i-j} \end{aligned}$$

In general, the correction term vanishes only when $N \rightarrow +\infty$, but we can ensure that it also vanishes for finite N by enforcing $I_n = 0$ for all $n \in \{N-M+1 \dots N-1\}$, i.e., there is no input current at the end of the stimulation. In the same way, $\langle I_{n-i} \rangle = \langle I_n \rangle$ for all $i \in \{0 \dots M-1\}$.

Then we define $a_k = \langle I_n I_{n-k} \rangle$ for all $k \in \{0 \dots M-1\}$, and $y = \langle I_n \rangle$, so

that the matrix \mathbf{A} can be written as follows:

$$\mathbf{A} = \begin{pmatrix} a_0 & a_1 & a_2 & \dots & a_{M-1} & y \\ a_1 & a_0 & a_1 & \dots & a_{M-2} & y \\ a_2 & a_1 & a_0 & \dots & a_{M-3} & y \\ \dots & \dots & \dots & \dots & \dots & y \\ a_{M-1} & a_{M-2} & a_{M-3} & \dots & a_0 & y \\ y & y & y & \dots & y & 1 \end{pmatrix} = \begin{pmatrix} \tilde{\mathbf{A}} & \mathbf{Y} \\ \mathbf{Y}^T & 1 \end{pmatrix}$$

We also define $\mathbf{X} = \begin{pmatrix} \mathbf{K} \\ V_0 \end{pmatrix}$ and $\mathbf{B} = \begin{pmatrix} \tilde{\mathbf{B}} \\ \langle V_n \rangle \end{pmatrix}$ and $\mathbf{Y}^T = (y \ y \ \dots \ y)$.

Solving the matrix equation by block gives

$$V_0 = \langle V_n \rangle - \mathbf{Y}^T \mathbf{K} = \langle V_n \rangle - \langle I_n \rangle \sum_{p=0}^{M-1} K_p$$

$$(\tilde{\mathbf{A}} - \mathbf{Y} \mathbf{Y}^T) \mathbf{K} = \tilde{\mathbf{B}} - \langle V_n \rangle \mathbf{Y}$$

The coefficients of the matrix $\mathbf{U} = \tilde{\mathbf{A}} - \mathbf{Y} \mathbf{Y}^T$ are $u_{i,j} = a_{|i-j|} - \langle I_n \rangle^2$. The coefficients of the vector $\tilde{\mathbf{B}} - \langle V_n \rangle \mathbf{Y}$ are $\langle V_n I_{n-i} \rangle - \langle V_n \rangle \langle I_n \rangle$. The matrix \mathbf{U} is a Toeplitz matrix, and solving a linear problem for a Toeplitz matrix can be done very quickly with the use of the Levinson-Durbin algorithm (which is documented for example in [6]).

It appears that it is not necessary to store all the values of V_n and I_n . The averages $\langle V_n I_{n-j} \rangle$ can be computed online in real time (M additions at each time step).

5.3 Choosing the input signal

The input signal I must be chosen so that

1. it is zero at the end of the stimulation (last M steps, where M is the kernel size) in order to use the Levinson-Durbin algorithm, as shown in the previous section;
2. the neuron response is essentially linear;
3. it makes the best possible use of the D/A converters of the acquisition board.

Constraint 2 is satisfied by letting (I_n) be a sequence of independent random numbers with appropriate variance. Constraint 3 is satisfied by letting each current step I_n be a random number with uniform distribution in the range of D/A converter. Thus, the input current is a stationary non-gaussian white noise (digitally sampled). We discuss this choice in the following.

Linearity of the membrane response

In general, the membrane potential does not respond linearly to the input current. However, it can be considered as locally linear around a given value of the potential; our strategy is thus to inject a signal that has a small effect on the membrane and a large effect on the electrode.

Because the electrode time constant is much smaller than the membrane time constant, the choice of a white noise input signal ensures that the membrane potential will not vary much while the electrode potential will vary much more. Indeed, the standard deviation of the response of a membrane with time constant τ_m and resistance R_m to a white noise is proportional to $R_m/\sqrt{\tau_m}$. Thus, if the electrode has time constants τ_e and resistance R_e then the ratio of electrode response over membrane response is

$$\frac{R_e}{R_m} \sqrt{\frac{\tau_m}{\tau_e}}$$

For a sharp electrode, the electrode and membrane resistances have the same magnitude and with a properly adjusted recording setup, $\tau_m \approx 100\tau_e$, so that the electrode voltage response is about 10 times larger than the membrane response. Thus it is possible to ensure that the membrane potential remains within about 1 mV of its resting potential while the recorded potential varies by 10 mV on average.

Besides, we remark that the linearity of the membrane response is not so crucial in the estimation procedure because in cases when the response is non-linear, the algorithm finds the best linear approximation (in the least square sense).

Determining the level of noise injection

To estimate the kernel K , we inject a noisy current consisting of a sequence of independent random current steps at sampling resolution Δ , with amplitude uniformly distributed between $-I_{\max}$ and $+I_{\max}$. I_{\max} is chosen so that the membrane potential remains close to its resting level, while the electrode response is large enough so as to maximize the signal/noise ratio. For an ideal electrode (i.e., very fast compared to the membrane), the membrane response is piecewise exponential, it is a low-pass filtered version of $R_m I(t)$ with time constant τ_m , where R_m is the membrane resistance, $I(t)$ is the injected current and τ_m is the membrane time constant. The standard deviation σ_V of the membrane potential is then given by the following formula:

$$\sigma_V = \sqrt{\frac{1 - e^{-\frac{\Delta}{\tau_m}}}{1 - e^{-\frac{\Delta}{\tau_m}}} R_m \sigma_I} \approx \sqrt{\frac{\Delta}{6\tau_m}} R_m I_{\max}$$

where σ_I is the standard deviation of the injected current, and assuming that the sampling step Δ is small compared to the membrane time constant τ_m . With the values $\Delta = 0.1$ ms, $\tau_m = 10$ ms, $R_m = 40$ M Ω and $I_{\max} = 0.5$ nA, we obtain $\sigma_V = 0.8$ mV, which is small enough. The expression we derived applies to an

ideal electrode; for non-ideal electrodes (which filter the injected current), it gives an upper bound for σ_V (approximately, τ_m is replaced by $\tau_m + \tau_e$, where τ_e is the electrode time constant). The electrode time constant is of the same order as the sampling step, therefore the electrode response can occasionally be close to the upper bound $R_e I_{\max}$, where R_e is the electrode resistance. It is crucial to estimate the range of the measured signal in order to adjust the acquisition system correctly. With $R_e = 50 \text{ M}\Omega$ and $I_{\max} = 0.5 \text{ nA}$, the range is $\pm 25 \text{ mV}$, which was appropriate for our acquisition system.

5.4 Isolation of electrode kernel

Once the kernel of the system neuron+electrode has been determined, the electrode kernel remains to be extracted. The idea is that the membrane is much slower than the electrode, so that we can distinguish the two contributions in the full kernel.

As a first approximation, we can write $K = K_m + K_e$, where K_m is the membrane kernel and K_e is the electrode kernel. We suppose that, in the regime in which the kernel was obtained (i.e., small white noise injection), the membrane responds approximately as a first order low-pass linear filter (i.e., a resistor-capacitor circuit), so that

$$K_m(t) = \frac{R}{\tau} e^{-t/\tau}$$

The electrode kernel is supposed to decay much faster, so that for large t , $K(t) \sim K_m(t)$. This suggests the idea of estimating K_m by fitting an exponential function to the tail of K and subtracting it ($K_e = K - K_m$).

However, a more careful examination of the circuit shows that the assumption $K = K_m + K_e$ is a crude approximation. Indeed, the recorded potential can be written as

$$\begin{aligned} V_r &= V_m + U_e \\ &= V_0 + K_m * I_m + K_e * I \end{aligned}$$

where V_m is the membrane potential (which is the quantity we want to recover), U_e is the potential across the electrode, and I_m is the current entering the membrane. The electrode filters the command current I ; a reasonable approximation is to set $I_m = U_e/R_e$, where $R_e = \int K_e$ is the electrode resistance (defined as the ratio U_e/I for a constant injected current I). It follows that the full kernel reads

$$K = K_m * \frac{K_e}{\int K_e} + K_e \quad (3)$$

Thus the membrane kernel cannot be simply subtracted from the total kernel. However we can still use the tail of K to estimate the membrane time constant.

Using the tail of the kernel to estimate the membrane time constant

We assume that the electrode kernel K_e decays faster than the membrane kernel, i.e., $K_e(t) = o(e^{-t/\tau})$. In fact, we expect that $K_e(t) \sim \alpha e^{-t/\tau_e}$ for large t , with $\tau_e < \tau_m$. For large t , we have:

$$\begin{aligned} K_m * \frac{K_e}{R_e} &= \frac{R}{R_e \tau} \int_0^t e^{\frac{s-t}{\tau}} K_e(s) ds \\ &\sim \frac{R}{R_e \tau} e^{-\frac{t}{\tau}} \int_0^{+\infty} e^{\frac{s}{\tau}} K_e(s) ds \end{aligned}$$

where the convergence of the integral is guaranteed by the dominated convergence theorem. Thus, fitting an exponential function to the tail of the kernel gives the correct membrane time constant, but not the correct membrane resistance (it overestimates the resistance). For example, for a simple RC electrode with resistance R_e and membrane time constant τ_e , we obtain

$$K_m * \frac{K_e}{R_e} = \frac{R}{\tau} e^{-\frac{t}{\tau}} \times \frac{\tau}{\tau - \tau_e}$$

It follows that the membrane resistance is overestimated by about $\frac{\tau_e}{\tau}$ (with $\tau_e \ll \tau$). Thus for a (very) good recording the error would be around 1%.

How to define the “tail” of the kernel?

The result above is an equivalent when t goes to infinity. In practice, we need to split the kernel K at some point T (the tail parameter) and to fit an exponential function to the right part (the “tail” of the kernel). The larger this point T is, the closer the tail is from the correct exponential function ($e^{-t/\tau}$), but the fewer data points are available for the fitting procedure. Thus, there is a compromise in the choice of T . A rule of thumb is that T must be at least 10 times the expected electrode time constant, while allowing the tail to contain at least one membrane time constant. Typical values in our experiments were $T \approx 3 - 5$ ms. Supplementary Figure 1 shows that only the magnitude of T is important, the procedure is not very sensitive to the precise value.

Removing the membrane kernel

We use equation (3) to extract the electrode kernel K_e from K . Here we assume that the membrane kernel K_m has already been recovered, i.e., the parameters R_m and τ_m are known. In the next section we explain how to obtain good estimates for these parameters, but for the moment we can assume that we have obtained the correct parameters.

First, we need to estimate the electrode resistance. We have $R_e = \int_0^{+\infty} K - R_m$. In practice only the first M steps of the kernel is known, so that the formula

we need is actually:

$$R_e = \int_0^{M\Delta} K - R_m + R_m^* e^{-\frac{M\Delta}{\tau_m}}$$

where Δ is the sampling step and R_m^* is the estimate from fitting an exponential function to the tail of the full kernel K .

Then we use the Z-transform to solve equation (3). Since convolutions are transformed into products, we obtain:

$$\mathcal{Z}[K_e] = \mathcal{Z}[K] \left(\frac{\mathcal{Z}[K_m]}{R_e} + 1 \right)^{-1}$$

We have

$$\mathcal{Z}[K_m] = R_m \frac{\Delta}{\tau_m} \frac{1}{1 - \lambda z^{-1}}$$

with $\lambda = e^{-\Delta/\tau_m}$. We define $\alpha = \frac{R_m \Delta}{R_e \tau_m}$ and after a little algebra, we obtain

$$\mathcal{Z}[K_e] = \mathcal{Z}[K] \left(1 - \frac{\alpha}{\alpha + 1} \frac{1}{1 - \frac{\lambda}{\alpha + 1} z^{-1}} \right)$$

The second term corresponds to a first order low-pass filter which can be implemented recursively as follows:

$$\begin{cases} Y_0 = \frac{\alpha}{\alpha + 1} K_0 \\ Y_n = \frac{\alpha}{\alpha + 1} K_n + \frac{\lambda}{\alpha + 1} Y_{n-1} \quad \text{for } n > 0. \end{cases}$$

then $K_e = K - Y$.

Optimizing the membrane parameters

The difficulty in using the procedure above is that only τ_m can be estimated from the tail of the kernel K , while it is hard to estimate R_m reliably. It follows from section 5.4 that if R_m is not estimated correctly, then the estimated electrode kernel K_e includes a residual slow component (e^{-t/τ_m}) from the membrane kernel. Therefore we use the following strategy to obtain a better estimate of R_m : for each value R_m^* of the membrane resistance, the procedure gives an estimate of the electrode kernel $K_e(R_m^*)$; for the true value $R_m^* = R_m$ we expect the residual slow component to vanish, so that we search the resistance value which minimizes the tail of $K_e(R_m^*)$:

$$R_m = \underset{R_m^*}{\operatorname{argmin}} \int_T^{+\infty} K_e(R_m^*)^2 dt$$

Since the variable to be adjusted is only one-dimensional, we simply use the golden search algorithm to find the optimal resistance. Note that the formula above is exact in the limit of large T .

5.5 Implementation

The computer implementation should follow easily from the algorithms we have previously described. In this section we outline a few important points and the general procedure. The programs must run on a real time computer system connected to the amplifier.

Estimation procedure

The estimation procedure lasts about 10 s and must be performed when the electrode is impaled in the neuron (because the properties of the electrode are not the same as in the extracellular medium). During this time, a uniform white noise current (in the form of a sequence of independent random numbers) is injected in the neuron. The signal is sent through an acquisition board to the amplifier. The amplifier should be properly set, with the capacitance neutralization circuit set at a high level (so as to reduce the time constant of the electrode). The bridge compensation circuit must be off. The range of the uniform noise must be the same as the range of the D/A converters of the acquisition board. The range of the input A/D converters, which relay the voltage recording to the computer, must be large enough to avoid clipping (it is best to check on an external oscilloscope). Although the membrane potential does not vary much, the electrode voltage is much more variable. For example, if the range of the uniform current is ± 1 nA and the electrode is very fast (i.e., faster than the acquisition rate) and its resistance is 100 M Ω (sharp electrode), then the potential would vary between -100 mV and 100 mV. Note that it can be useful to change the offset of the voltage output of the amplifier so that the resting potential is close to 0 mV.

The computer program does not need to store the whole sequence of measures (I and V). It is enough so store in memory the running averages of $I_n I_{n-i}$, $V_n I_{n-i}$, I_n and V_n . At the end of the stimulation, the program applies the Levinson-Durbin algorithm to find the full kernel and extract the electrode kernel with the algorithms described previously (exponential fitting of the tail followed by suppression of the membrane kernel). This part of the algorithm is not required to run in real time. Subsequently, only the electrode kernel needs to be stored. Typically, the resulting kernel is short and only the first tens of steps are non zero.

Online compensation

Once the electrode kernel has been calculated, it can be used in real time to estimate the electrode voltage and subtract it from the recording. Again, the bridge compensation circuit must be turned off on the amplifier. Then it must be remembered that the potential actually recorded by the system is the sum of the membrane and the electrode responses and therefore it can be much larger than the membrane potential. The electrode voltage is subtracted in real time by a convolution, the

input current I being known:

$$V_m(n) = V_r(n) - \sum_{p=0}^{l-1} K_e(p)I(n-p)$$

where l is the number of steps in the electrode kernel (typically 30–50). Thus, the value of the previous l steps of the injected current must be held in memory.

6 Typical sources of error

Here we enumerate a number of anomalous situations that can occur during the estimation or compensation stages, that may produce unwanted biases in the electrode kernel estimate. Many of these errors can be easily noticed as anomalies in the electrode kernel.

The bridge compensation is on: in this case the program can still capture a kernel but it has a strange shape with a total resistance close to 0 (if it is well adjusted), which makes the membrane suppression procedure fail.

Input or output ranges on the acquisition board are not correctly set: if the ranges are too large, the method only loses some accuracy; however if the ranges are not large enough, then clipping occurs, which can be disastrous both at the estimation stage and at the compensation stage. It can remain unnoticed at the estimation stage because it only results in errors in the estimated kernel. At the compensation stage it results in large compensation errors which can be seen as noise on the compensated output in current clamp. It is more serious in dynamic clamp because it can result in losing the cell because of oscillatory instabilities.

The kernel is too large: if the number of steps M in the full kernel is very large, then during the estimation procedure the program may not have enough time to compute all the running averages within one time step. Depending on the real time system, this can result in freezing the program or in errors in the kernel. The latter is more problematic because it can remain unnoticed: in this case, the program sometimes takes more than one step to do all the required operations and it can be an important source of error. Therefore it is important to check that the kernel is not too large for the system.

The tail parameter is too small: one must specify what part of the kernel (which we called the tail) is used for estimating the membrane contribution. If the splitting time is too small, then the tail contains part of the electrode kernel, which makes the procedure fail. This can sometimes be seen as a negative part appearing in the electrode kernel (usually the kernel is entirely positive).

The tail parameter is too large: if the splitting time is too large, then remaining tail is too small to estimate the membrane kernel reliably. This also results in errors in the electrode kernel (although not as serious). There is however a broad range of values of this parameter for which there is no significant error in the kernel (Supplementary Figure 1).

The capacitance neutralization has changed: it must be remembered that the electrode kernel captures in fact not only the electrode properties, but the properties of the whole recording setup, including the amplifier. Therefore if any circuit is used on the amplifier, their setting must remain unchanged as long the same electrode kernel is used, otherwise the estimation procedure should be run again.

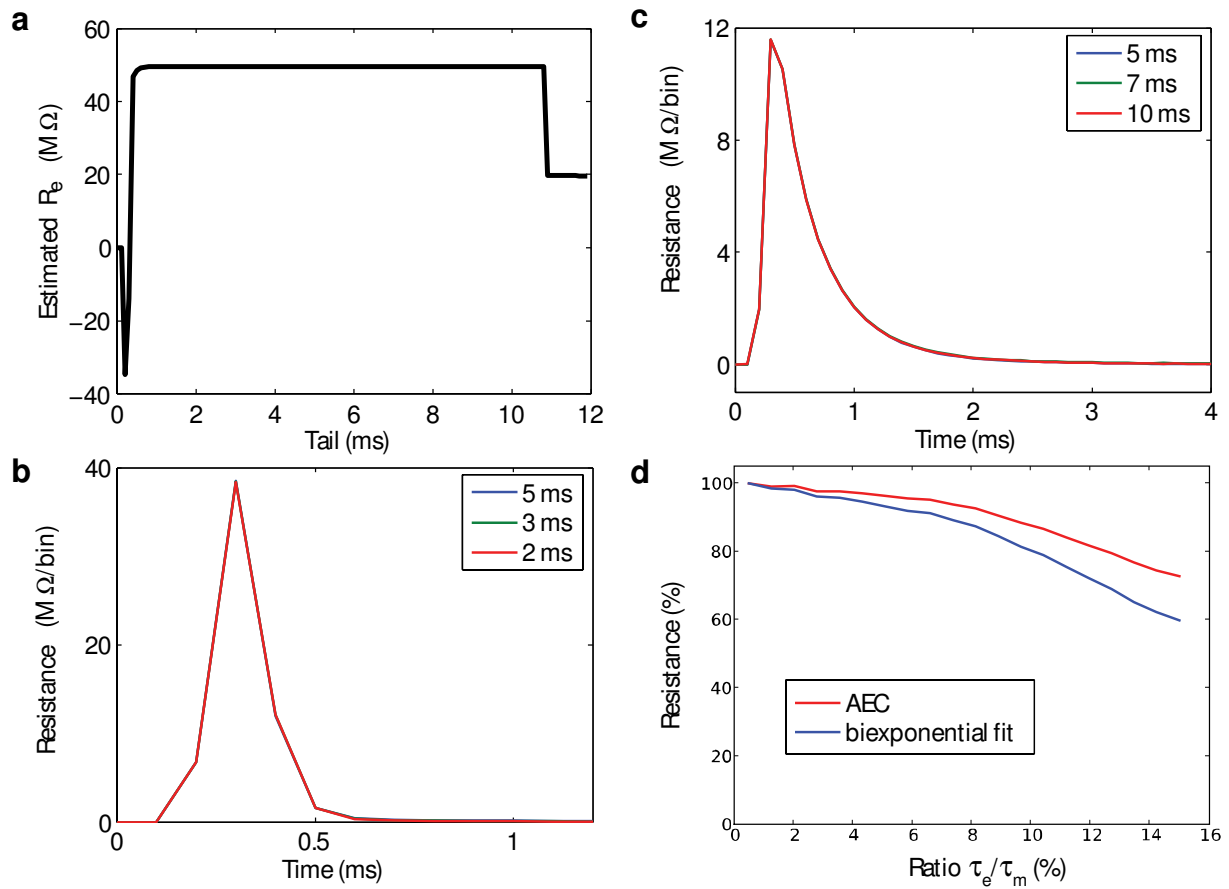
The electrode properties have changed: it happens that the electrode properties change during an experiment for some reason (e.g. small movements of the electrode). It results in compensation errors which can be seen as abnormal noise on the traces (with current noise injection). In this case the estimation procedure must be run again (just like with the standard bridge compensation method). The best practice is to run the estimation once in a while in order to check that the electrode properties have not changed.

References

- [1] Rudolph, M., Piwkowska, Z., Badoual, M., Bal, T. and Destexhe, A. A method to estimate synaptic conductances from membrane potential fluctuations. *J. Neurophysiol.* 91, 2884-96 (2004).
- [2] Pospischil, M., Piwkowska, Z., Rudolph, M., Bal, T. and Destexhe, A. Calculating event-triggered average synaptic conductances from the membrane potential. *J. Neurophysiol.* 97, 2544-52 (2007).
- [3] Hines, M.L. and Carnevale, N.T. The NEURON simulation environment. *Neural Comput.* 9, 1179-209 (1997).
- [4] Destexhe, A., Rudolph, M., Fellous, J. M. and Sejnowski, T. J. Fluctuating synaptic conductances recreate in vivo-like activity in neocortical neurons. *Neuroscience* 107, 13 (2001).
- [5] Destexhe, A. and Rudolph, M. Extracting information from the power spectrum of synaptic noise. *J. Comput. Neurosci.* 17, 327-345 (2004).
- [6] Press, W. H., Flannery, B. P., Teukolsky, S. A. and Vetterling, W. T. *Numerical Recipes in C: The Art of Scientific Computing* (Cambridge University Press, 1993).

- [7] Azouz, R. and Gray, C.M. Dynamic spike threshold reveals a mechanism for synaptic coincidence detection in cortical neurons in vivo. Proc. Natl. Acad. Sci. USA 97, 8110-5 (2000).
- [8] Finkel, A. S., and Redman, S. Theory and operation of a single microelectrode voltage clamp. J Neurosci Methods 11, 101-127 (1984).

Supplementary Figure 1 - Sensitivity of electrode kernel to estimation parameters

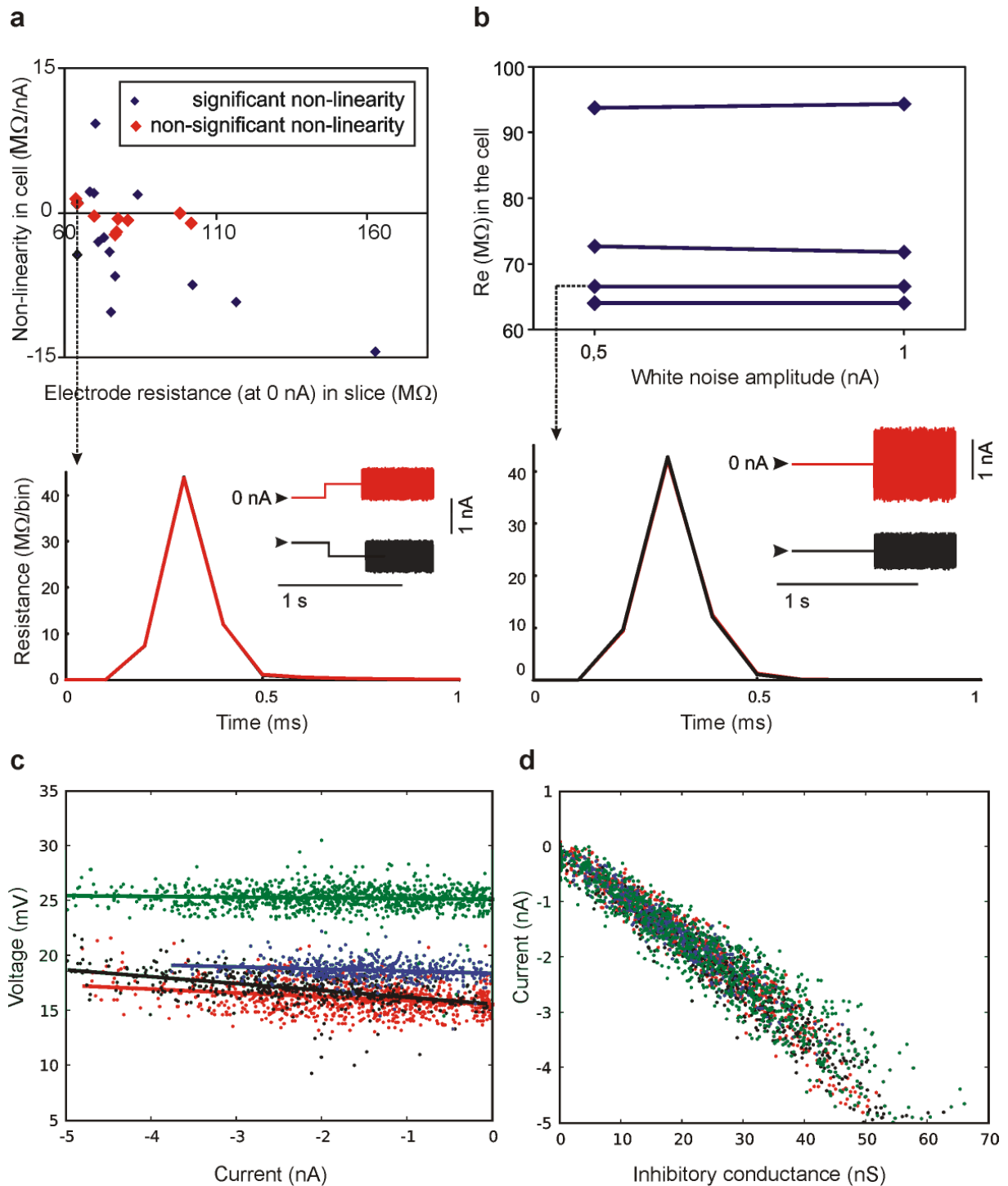


We tested the sensitivity of the electrode kernel estimation to the precise choice of the Tail parameter and to the ratio of time constants (τ_e/τ_m): the Tail parameter corresponds to the time from which the full kernel is considered as corresponding to the membrane response only, and it has to be chosen prior to the separation of the full kernel into a membrane kernel and an electrode kernel. **(a)** Simulations show that there is a broad plateau for which the kernel estimation is correct, as represented here by a plot of estimated electrode resistance R_e vs. Tail parameter (target $R_e = 50$ M Ω , electrode time constant $\tau_e = 0.2$ ms, membrane time constant $\tau_m = 15$ ms). If Tail is too small, part of the electrode kernel is removed together with the membrane kernel and estimated R_e is too small (left). If Tail is too close to the total size of the full kernel (15 ms in this case), the fit of the membrane response by an exponential fails and this also leads to a wrong estimation (right). **(b, c)** Two examples of real electrodes, showing that the estimated kernels are very similar for 3 different values of Tail used in each case, confirming the existence of a broad plateau (b: typical electrode with full capacitance compensation, $R_e = 62$ M Ω , RS cell; c: less capacitance compensation is used, the electrode is slower, $R_e = 59$ M Ω , RS cell). In 6 systematic comparisons (5 electrodes) of kernels estimated for Tail = 5 ms vs. Tail = 3 ms, the difference $R_{e_{5ms}} - R_{e_{3ms}}$ was of 1.4 M Ω only on average (range 0.5-2.3 M Ω), and in 7 comparisons (6 electrodes) of kernels estimated for Tail = 5 ms vs. Tail = 2 ms, the difference $R_{e_{5ms}} - R_{e_{2ms}}$ was similarly of 1.4 M Ω on average (range 0.7-2.3 M Ω). In these experiments, R_e was between 59 and 108 M Ω . **(d)** Simulations show that the quality of the electrode kernel degrades continuously when the ratio of electrode time constant and membrane time constant increases. The model included a passive membrane ($R_m = 50$ M Ω , $\tau_m = 20$ ms) and a simple

RC electrode with resistance $R_e = 80 \text{ M}\Omega$ and varying time constant. The red line is the estimated resistance with AEC, relative to the actual resistance ($80 \text{ M}\Omega$); the blue line is the estimated resistance from a bi-exponential fit – a standard procedure for bridge balance, see e.g. Anderson, Carandi and Ferster 2000 (J Neurophysiol 84 (2), 909-926). The error on estimated resistance with AEC was less than 10% for $\tau_e/\tau_m < 9\%$ (as a comparison, proper operation of discontinuous current-clamp requires $\tau_e/\tau_m < 1-2\%$).

In addition, for 3 electrodes in vitro, we tested the impact of the duration of white noise injection on the electrode kernel estimation (not shown). We found no significant difference between injections of 5, 10 or 20 s duration, when comparing, for each electrode, kernel parameters obtained during repeated white noise injections of different durations. For one electrode, 1 s white noise injections provided significantly different kernel parameters, compared to 5, 10 and 20 s injections (ANOVA followed by post hoc PLSD Fischer test, $P < 0.001$). We used 5 s of white noise injection in most subsequent experiments in vitro.

Supplementary Figure 2 – Electrode nonlinearity



(a) Top: For 20 electrodes (in 23 cells), we estimated the electrode resistance R_e from kernels obtained in the cell and in the slice at positive, zero and negative levels of constant injected current (positive current: 0.35 ± 0.1 nA depending on the cell, negative current: -0.5 ± 0.05 nA), by running the kernel estimation procedure. We used the slope of the linear regression between injected current and R_e *in the cell* to quantify the degree of nonlinearity. The nonlinearity is shown on the figure as a function the electrode resistance in the slice (measured before impalement). Each point

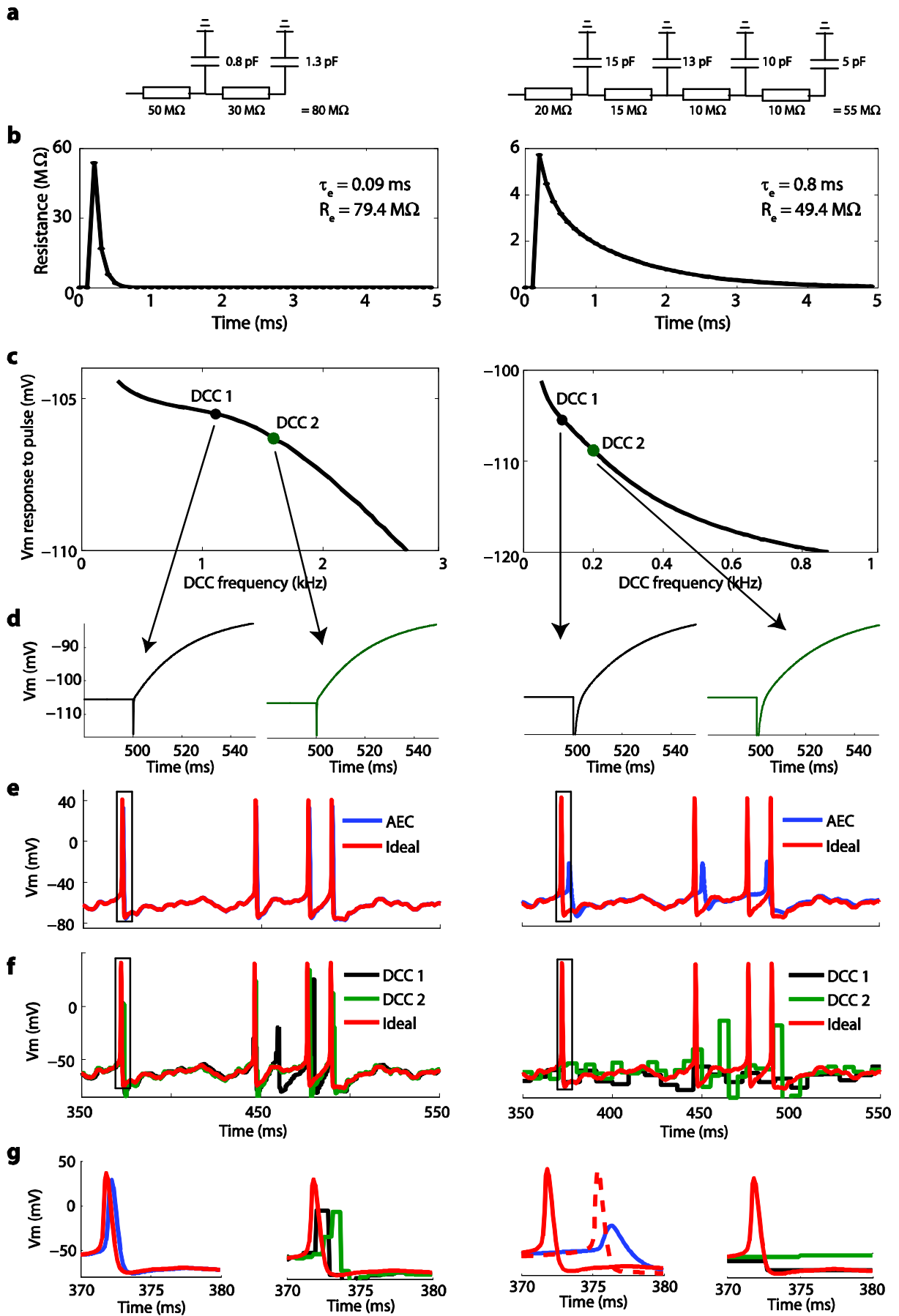
on the graph is one electrode tested in one cell (a small subset of electrodes was tested in more than one cell: each such test is one point). For 9 electrodes, we found that the linear regression slope was not significantly different from 0 (red points on the graph; two-tailed t-test), meaning that the current-dependent variability of the electrode resistance was comparable to the intrinsic variability of the electrode resistance (for these electrodes, the linear regression slope was $-0.5 \pm 1.1 \text{ M}\Omega/\text{nA}$). The few electrodes with unusually high resistance in the slice ($> 110 \text{ M}\Omega$) were very non-linear in the cell, which is consistent with standard physical interpretations of nonlinearities (RD Purves, Microelectrode methods for intracellular recording and iontophoresis, Academic Press, 1981). Bottom: an example of two kernels obtained for the same electrode using -0.4 nA (black) and $+0.4 \text{ nA}$ (red) of constant current in addition to the white noise injection. The resistance is 65.8 and $66.4 \text{ M}\Omega$, respectively.

(b) Top: For 3 electrodes (in 4 cells), we compared kernels obtained using white noise current injection ranging between -0.5 and $+0.5 \text{ nA}$ with kernels obtained using white noise current injection between -1 and $+1 \text{ nA}$. R_e for all these kernels is shown here, with lines connecting measurements obtained for the same electrode and cell. Bottom: an example of two kernels obtained for the same electrode using white noise current injection ranging between -0.5 and $+0.5 \text{ nA}$ (black), or between -1 and $+1 \text{ nA}$ (red). The electrode resistance is $66.5 \text{ M}\Omega$ in both cases.

(c) We analyzed the spikes produced by 4 cells during injection of colored conductance noise in vitro (as shown in Fig 1C). Because of the dynamic clamp protocol, a very large negative current was injected during spikes: $-1.6 \pm 1.1 \text{ nA}$ (red), $-2.4 \pm 1.1 \text{ nA}$ (black), $-1.4 \pm .7 \text{ nA}$ (blue) and $-1.9 \pm 1.1 \text{ nA}$ (green). Any error ΔR_e in the estimation of the electrode resistance, which could be caused by electrode nonlinearities during these large current injections, would result in an error $\Delta R_e \cdot I$ in the voltage estimation. For these cells, the voltage peak was not very variable (standard deviations 1.3 mV (red), 1.4 mV (black), 0.9 mV (blue) and 1.1 mV (green)), and the estimated resistance errors from linear regression between the injected current and the voltage at peaks were $-0.3 \text{ M}\Omega$ (red), $-0.6 \text{ M}\Omega$ (black), $-0.2 \text{ M}\Omega$ (blue), $-0.1 \text{ M}\Omega$ (green), which indicates an absence of fast nonlinearities. Electrode resistances ranged between $63 \text{ M}\Omega$ and $68 \text{ M}\Omega$ (estimated at rest with AEC).

(d) Because of the dynamic clamp protocol, the injected current was defined as a function of the voltage ($I = g_e(E_e - V) + g_i(E_i - V)$), which introduces a negative correlation between I and V that could have contaminated our results. However at spike peaks that correlation is weak because the excitatory current is almost zero and the total injected current is mainly determined by the inhibitory conductance (which is independent of V). This graph shows that this was indeed the case for the 4 cells (the resistance error estimated from the linear regression between $g_i(E_i - V)$ and V was even smaller: $-0.3 \text{ M}\Omega$, $-0.5 \text{ M}\Omega$, $-0.1 \text{ M}\Omega$, $-0.02 \text{ M}\Omega$).

Supplementary Figure 3 – Numerical simulation of conductance noise injection with AEC and DCC.



Left column : with a fast electrode made of two resistors and capacitors (time constant 0.09 ms from exponential fit); right column: with a slow electrode made of four resistors and capacitors (time constant 0.8 ms). The electrode is impaled into a cortical cell modeled as a single-compartment Hodgkin-Huxley type model (equations and parameters in Destexhe et al, J Neurophysiol 79 (1998), 999-1016), and connected to a model amplifier (emulating DCC, bridge compensation and an acquisition board; we used a model of the electrode previously published in a conference proceedings - Brette et al, Neurocomputing 70 (10-12), 1597, proceedings of CNS 2006, Edinburgh, UK). Programs were written in C++, differential equations were integrated with a second-order Runge-Kutta method (time step 1 μ s).

a) Electrical circuit of the electrode. The time constant of the fast electrode corresponds to our measurements in vitro (with full capacitance neutralization).

b) Electrode kernel estimated in the cell with AEC, and estimation of the electrode resistance (0.75% error for the fast electrode, 10% error for the slow electrode).

c) Vm response in DCC mode to a -0.4 nA current pulse lasting 400 ms as a function of the DCC frequency. DCC 1 is the optimal setting (left: 1.1 kHz, right: 0.11 kHz) for which the recorded response corresponds to the true intracellular Vm. The optimal DCC period is typically 8-10 times the electrode time constant. DCC 2 is a slightly higher setting, which corresponds to an underestimation of the electrode resistance (left: 1.6 kHz, $R_e = 78 \text{ M}\Omega$; right: 0.2 kHz, $R_e = 47.5 \text{ M}\Omega$). With the fast electrode, the inflexion point is close to the optimal setting but is not identical; with the slow electrode, there is no inflexion point.

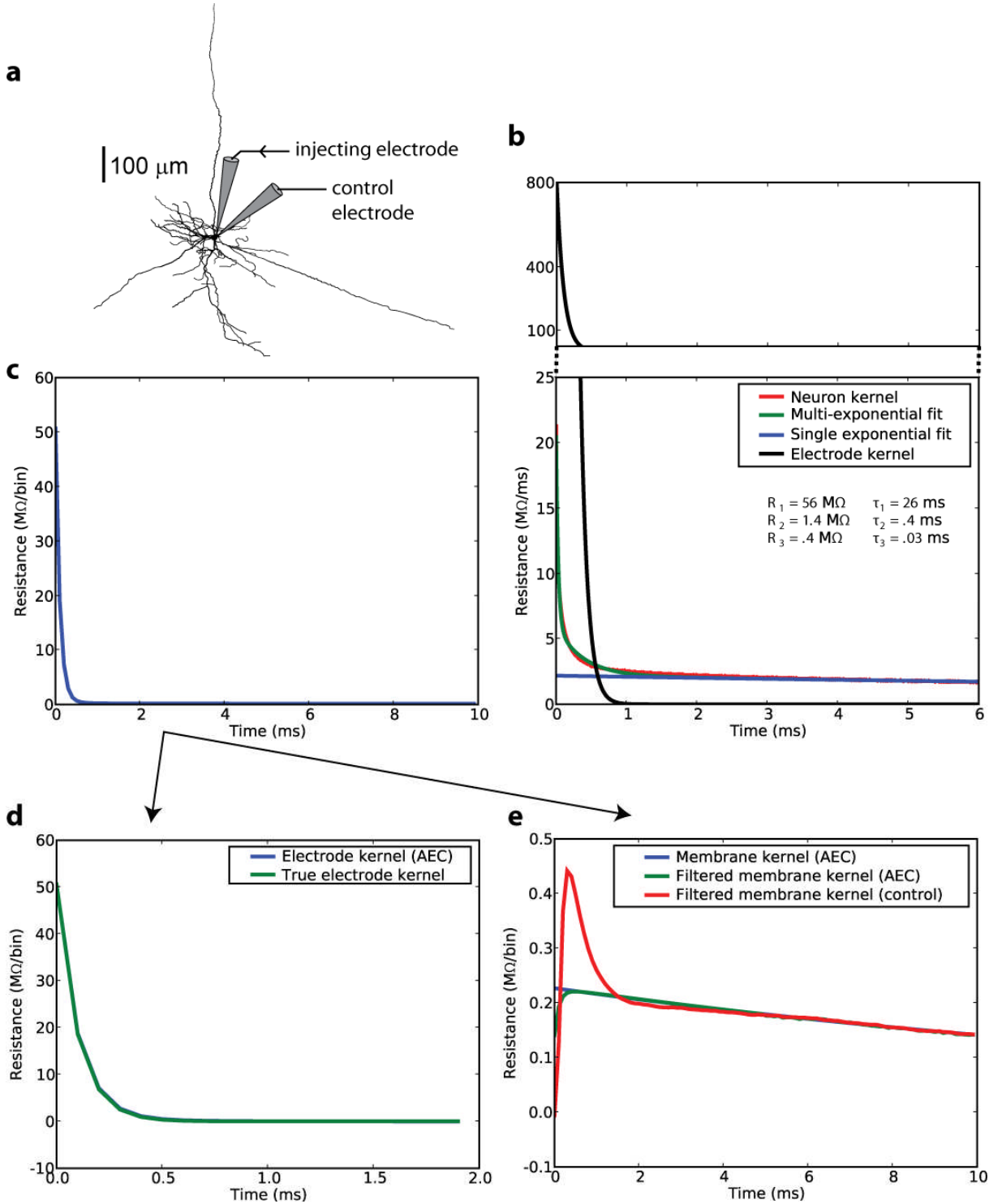
d) Bridge balancing traces for the corresponding settings (Vm recording of a pulse response using bridge compensation, i.e., estimating the electrode response as $R_e \times I(t)$). Black = optimal setting (perfect bridge compensation), green = higher setting, i.e., underestimation of the resistance. With the fast electrode, the non-optimal setting is hard to distinguish from the optimal one; with the slow electrode, it is not possible.

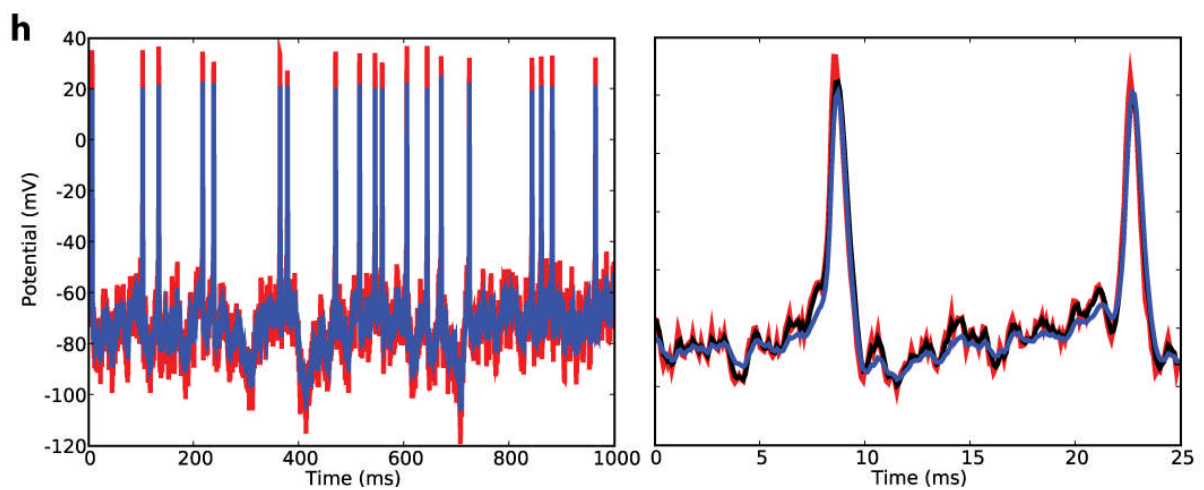
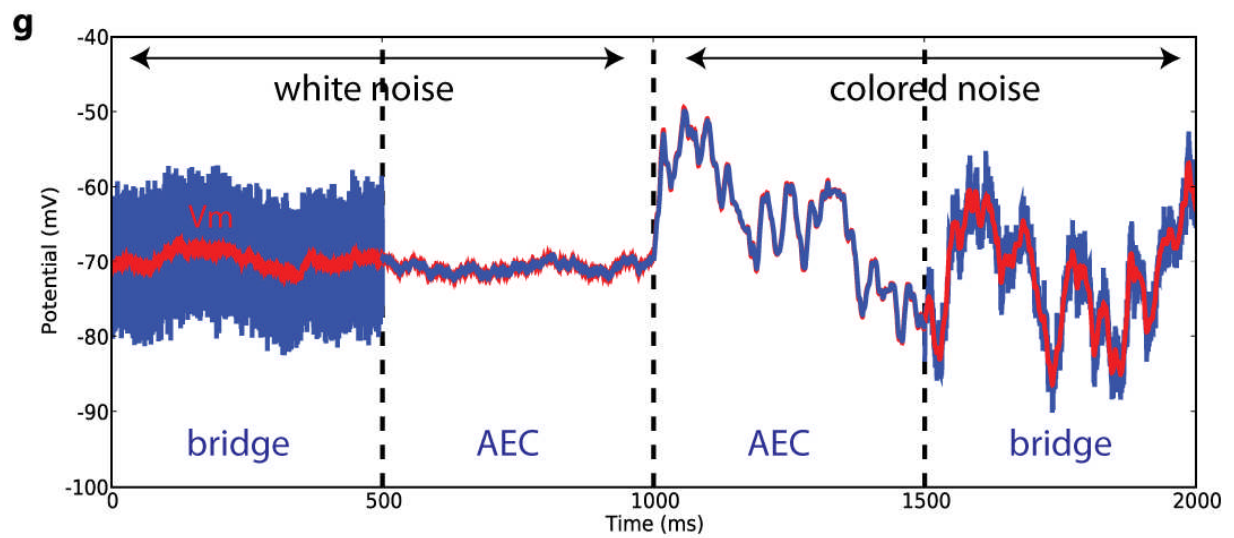
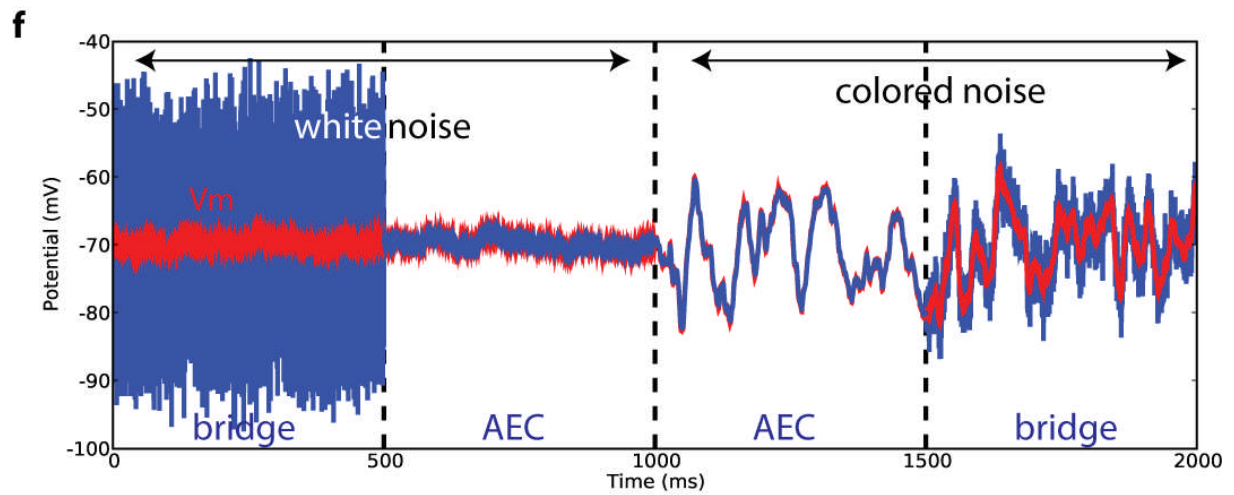
e) Response to a conductance noise injection (see main text) using AEC in dynamic-clamp. The red trace is the ideal recording with a zero-resistance electrode; the blue trace is the recording with AEC. The spike in the rectangle is enlarged in (g). With the fast electrode, both the subthreshold response and spikes are obtained with an excellent quality. With the slow electrode, the subthreshold response is good and spikes are recorded, but in a filtered version (see (g)).

f) Response to the same injection with DCC in dynamic-clamp. With the fast electrode, subthreshold responses are approximately correct (but a low temporal resolution and high-frequency noise) but spikes are missed or distorted. Besides, the setting which was optimal for current pulses (DCC 1) does not seem optimal for nonlinear events. With the slow electrode, both recordings are meaningless. Increasing the DCC frequency leads to unstable oscillations like in bridge (not shown).

g) Zoom on spikes (enlargement of rectangles in (e) and (f)). With the fast electrode, spikes recorded with AEC are very well reproduced with a slight filtering, while spikes recorded with DCC are very distorted due to the low temporal resolution. With the slow electrode, spikes recorded with AEC are filtered and delayed. The delay is also present in the cell (dashed red line = real Vm during AEC recording) and is due to a higher injected current (because the electrode resistance is underestimated); it does not appear in current clamp mode (not shown). Spikes cannot be recorded with DCC. Thus AEC recordings are possible with a slow electrode (equivalently, with a fast membrane) where DCC fails.

Supplementary Figure 4 – Simulations of AEC with morphologically reconstructed neurons





We simulated a morphologically reconstructed layer VI pyramidal cell (Contreras and Destexhe, *J Neurophysiol* 78 (1997), 335-350) using Neuron, with passive properties (b-g) as in Destexhe and Pare (*J Neurophysiol* 81 (1999), 1531-1547), compatible with whole-cell patch recordings: leak conductance $g_l = 0.0155 \text{ mS/cm}^2$ (range tested: $0.015\text{-}0.03 \text{ mS/cm}^2$),

resting potential $V_{rest} = -80$ mV, intracellular axial resistivity $R_a = 70$ Ω .cm (range tested: 65-280 Ω .cm), specific membrane capacitance $c_m = 1$ μ F/cm². In the simulations of panel h, voltage-dependent Na⁺ and K⁺ currents were inserted in soma, dendrites and axon (parameters in Destexhe and Pare, 1999). Two electrodes, modeled as a resistor and a capacitor, were located into the soma. White noise and colored noise currents were injected through the first electrode and AEC was used to correct the recording; the second electrode only recorded the membrane potential and served as a control. AEC and subsequent analysis were done offline using custom Python code (<http://www.di.ens.fr/~brette/HRCORTEX/AEC/>) and the Brian simulator (<http://brian.gforge.inria.fr/>). Recordings were sampled at 10 kHz (Neuron simulations use a 0.01 ms integration time step).

(a) Dendritic tree of the simulated neuron, reconstructed from a layer VI pyramidal cell (Contreras and Destexhe, 1997). Two electrodes are located into the soma. The intracellular resistivity was 70 Ω .cm (Stuart and Sprutson, J Neurosci (1998) 18, 3501-3510) in all simulations shown here. Each electrode was modeled as a resistor and a capacitor, with $R_e = 80$ M Ω and $\tau_e = .1$ ms (sharp electrodes) in all figures except (g), where $R_e = 20$ M Ω and $\tau_e = .5$ ms (patch electrodes, with a resistance typical of in vivo recordings). For sharp-electrode simulations, an additional leak conductance of 10 nS was inserted in soma to model the impalement, making the membrane time constant shorter (26 ms) compared to patch-electrode simulations (67 ms).

(b) The impulse response (kernel) of the cell with somatic injection (red) was fitted to a sum of three exponential functions (green):

$$\text{Fit}(t) = (R_1/\tau_1)\exp(-t/\tau_1) + (R_2/\tau_2)\exp(-t/\tau_2) + (R_3/\tau_3)\exp(-t/\tau_3)$$

with the values shown in the figure (the kernel was calculated with $dt = 0.01$ ms and the result is shown in M Ω /ms). The largest component (single exponential, blue) accounts for 56 M Ω of the total resistance $R = 57.8$ M Ω . The electrode kernel (black) is concentrated on the first ms and is two orders of magnitude larger than the membrane kernel on that time scale (note the change of scale in the upper part of the figure). The neuron and electrode kernels were calculated separately, i.e., the neuron kernel was estimated with no electrode resistance, and the electrode kernel was calculated without the neuron (therefore, it is a single exponential function with time constant .1 ms); thus, these calculations did not rely on AEC.

(c) Full kernel K (neuron + electrode) calculated from white noise injection through the first electrode located into the soma (displayed in M Ω /bin, with .1 ms bins).

(d-e) The full kernel was separated between electrode (d) and membrane (e) kernels with AEC (as described in the main text). The recovered electrode kernel (d, blue) was very close to the real one (d, green); the estimation gave $R_e = 81$ M Ω instead of 80 M Ω . The decomposition method assumes that the membrane kernel is a single exponential (e, blue),

so that the kernel of the AEC compensated recording $K - K_e$ is a filtered version of that exponential function (e , green). There is a significant difference with what the second electrode sees from the membrane at short time scales (e , red, full kernel with respect to injection in electrode 1 and recording in electrode 2), but that difference remains very small compared to the electrode resistance on the same time scale (d).

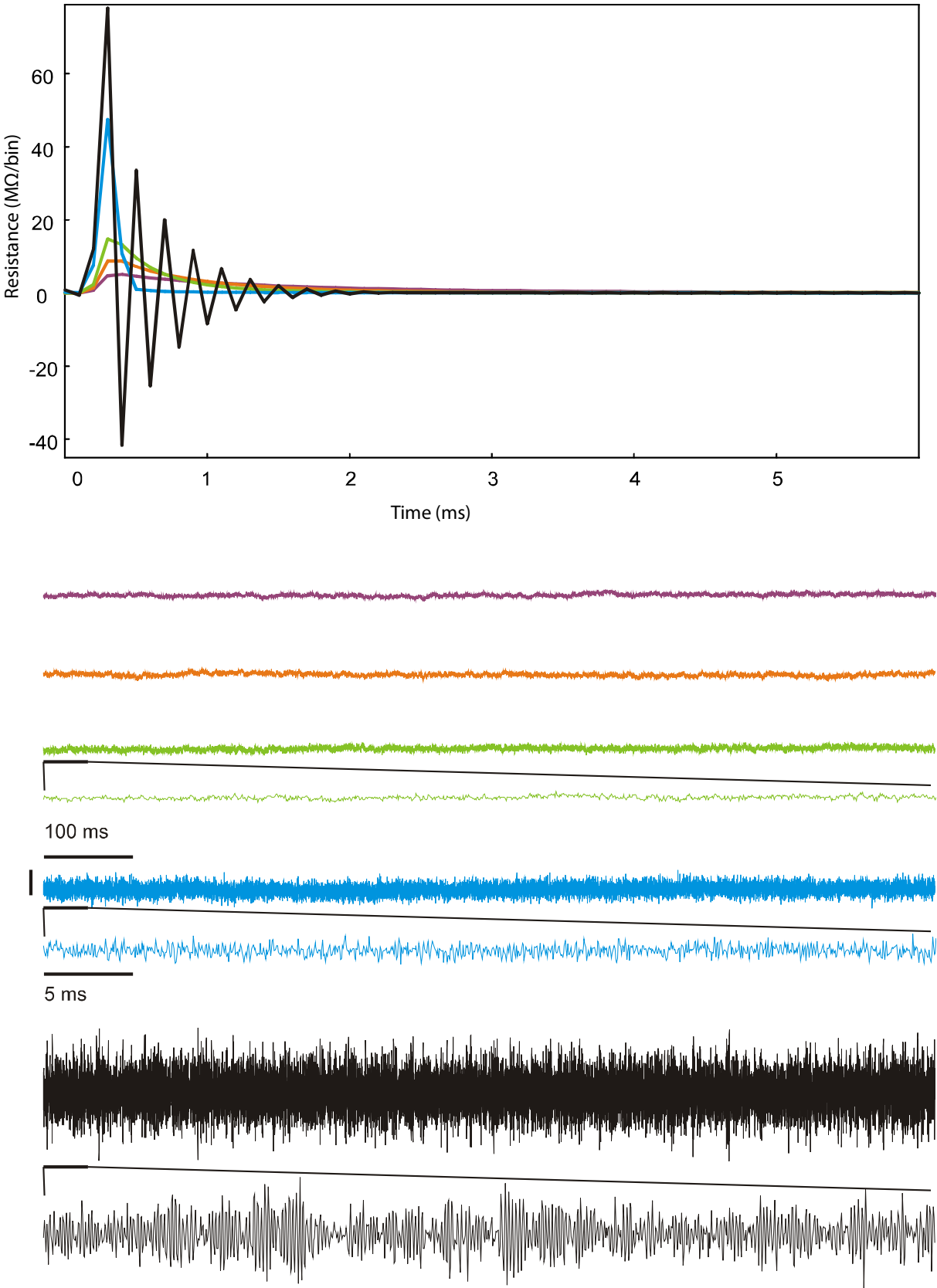
(f) The electrode kernel shown in (d) was used to compensate the recording (from the injecting electrode) while injecting white noise (1st second; sequence of independent 0.1 ms current steps uniformly distributed between -0.5 nA and 0.5 nA) and colored noise (2nd second; standard deviation 0.3 nA, time constant 5 ms). The AEC compensated trace (blue, $500 - 1500$ ms) is compared to the bridge compensated trace (blue, $0 - 500$ ms and $1500 - 2000$ ms) and to the real somatic potential of the model (red; the trace is switched from foreground to background between 500 ms and 1500 ms to avoid masking).

(g) The sharp electrodes were replaced by patch electrodes with resistance 20 M Ω and time constant 0.5 ms, and the leak current modeling the bad seal was removed. Consequently, the cell impulse response at the soma was fit by a sum of three exponential functions with $R_1 = 140$ M Ω , $R_2 = 1.6$ M Ω , $R_3 = 0.5$ M Ω , $\tau_1 = 63$ ms, $\tau_2 = 0.47$ ms and $\tau_3 = 0.03$ ms (thus, the main change is in the largest exponential term). The simulations are otherwise the same as in (f). The electrode resistance estimation was 20.6 M Ω instead of 20 M Ω .

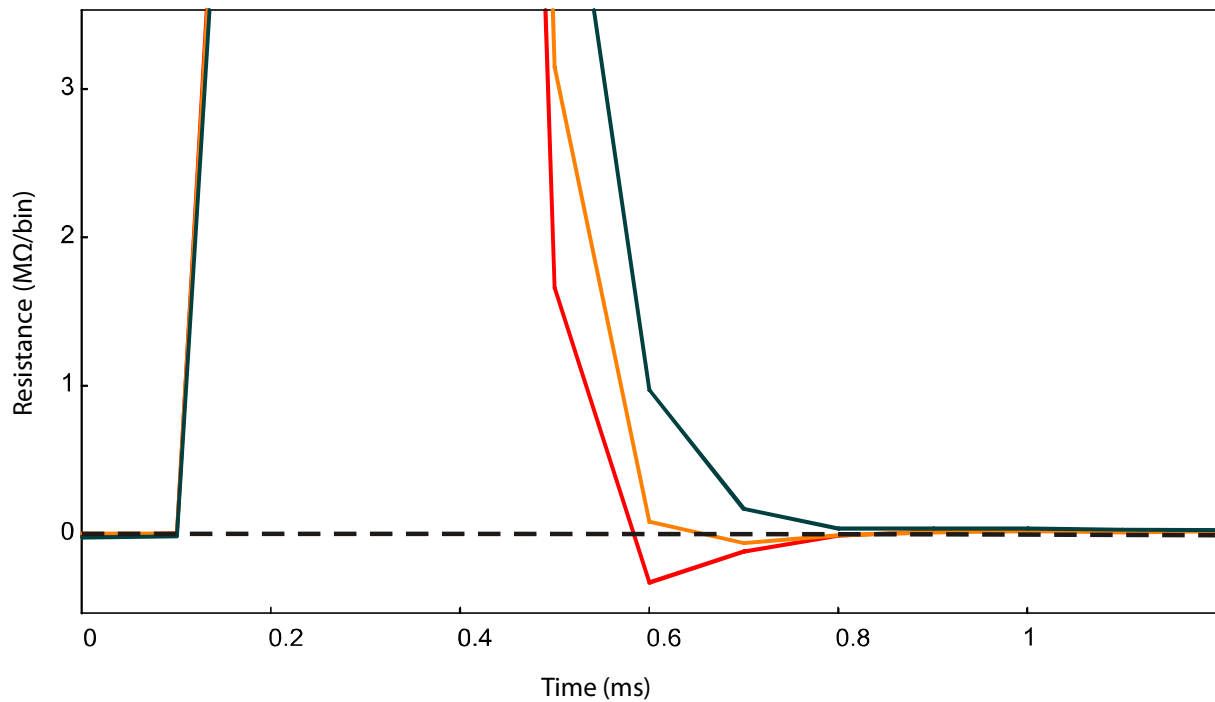
(h) This figure shows a very challenging situation for electrode compensation: nonlinear voltage-dependent conductances in the cell, electrode kernel estimated during spiking activity, large dendritic contributions to the membrane kernel, high ratio electrode resistance / membrane resistance, short membrane time constant and white noise injection. Voltage-dependent conductances were inserted, so that the cell was able to produce action potentials. Sharp electrodes were inserted in the soma as in (c-f). As a result, the membrane resistance (and thus the time constant) at rest was halved (and even more reduced during spiking), giving a large ratio $R_e/R_m = 2.5$ (even larger during spiking activity: R_e/R_m). Suprathreshold white noise was injected through the electrode, inducing spiking activity. The electrode kernel was estimated with the same suprathreshold white noise injection, i.e., there were spikes during the estimation. The estimated electrode resistance was 82.6 M Ω , which was very close from the same estimation with subthreshold white noise injection (estimated $R_e = 82$ M Ω). The blue trace shows the result of AEC compensation during the injection (red = real somatic potential). Even though the subthreshold activity looks filtered by AEC because the fast dendritic contribution to the membrane kernel is large (10% at rest), the technique does not act as a low-pass filter: action potentials are no more filtered than what is seen at the control (non-injecting) electrode (black).

Supplementary Figure 5 – Fine-tuning the capacitance neutralization with AEC

a



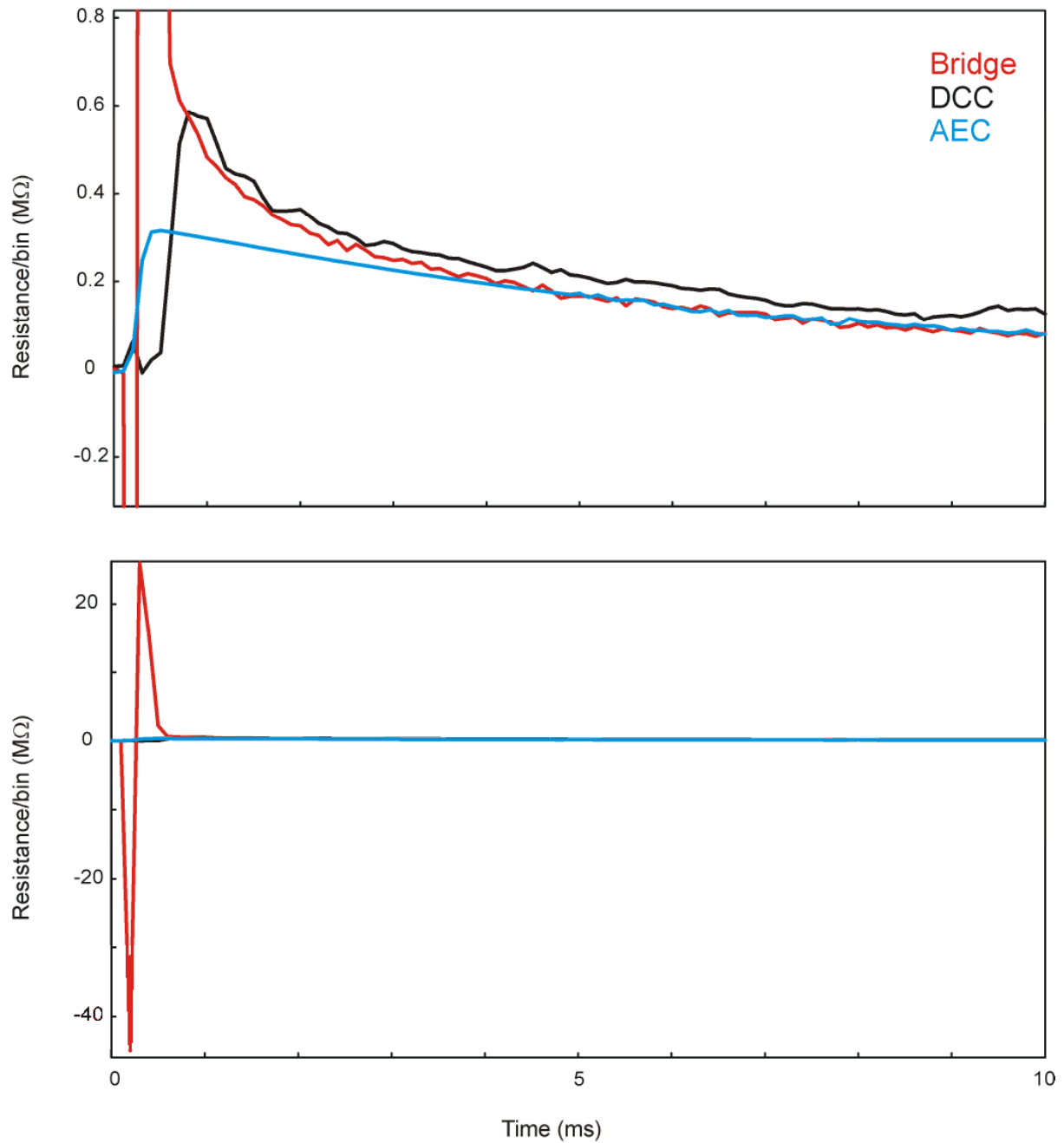
b



(a) Top: kernels obtained for one electrode, in the slice, at different levels of capacitance compensation. Bottom: Corresponding baseline traces recorded at each capacitance compensation level. The blue kernel and trace are one example of the maximal capacitance compensation setting that we used in this study. The black kernel and trace show a very clear example of oscillations due to capacitance overcompensation, seen at the level of the trace as well as at the level of the electrode kernel.

(b) A zoom on three electrode kernels obtained for slightly different levels of capacitance compensation in the same cell. The black kernel corresponds to the lowest capacitance compensation level of the three, which is the one that is chosen here for further recording. The red and orange kernels, on the other hand, display a small undershoot corresponding to a dampened oscillation, i.e. a slight over-compensation of the capacitance, and are discarded. The careful observation of the kernels thus allows the precise tuning of the capacitance compensation setting.

Supplementary Figure 6 – Correlation function between injected current and Vm (bridge compensation, DCC and AEC).



The membrane response to white noise injection was recorded in the same cell with three different compensation procedures: bridge compensation, DCC and AEC, and the correlation function between injected current and recorded voltage is plotted above (bottom: larger vertical scale). For AEC, it corresponds to the difference between the full kernel and the electrode kernel (which are obtained with white noise injection). With AEC, the correlation function appears as a filtered exponential function, as expected. With bridge compensation, the same transients as can be seen in response to pulses also appear in the correlation function. With DCC, the correlation function seems to be globally overestimated in this example, illustrating the difficulty of finding the perfect DCC settings.